

# CRISPR-based Herd Immunity Limits Phage Epidemics in Bacterial Populations

Pavel Payne<sup>1,3,\*</sup>, Lukas Geyrhofer<sup>2</sup>, Nicholas H. Barton<sup>1</sup>, Jonathan P. Bollback<sup>3,1</sup>

**1** Institute of Science and Technology Austria, Am Campus 1, Klosterneuburg, Austria

**2** Technion – Israel Institute of Technology, Haifa, Israel

**3** Institute of Integrative Biology, University of Liverpool, Liverpool, UK

\* E-mail: [pavel.payne@liverpool.ac.uk](mailto:pavel.payne@liverpool.ac.uk)

Short title: CRISPR-based Herd Immunity in Bacteria

Keywords: CRISPR, herd immunity, phage, bacteriophage, T7, bacteria, epidemic, polymorphism

## Abstract

Pathogens are a driving force in evolution, giving rise to a diversity of host immune defenses. In order for a pathogen to spread in a population a sufficient number of its members must be susceptible to infection, as resistant individuals can prevent the spread of a pathogen among susceptible hosts in a process known as herd immunity. While herd immunity has been extensively studied in vertebrate populations, little is known about its role, if any, in the dynamics between bacteria and their phage pathogens. Here we explore the dynamics of T7 phage epidemics in structured and unstructured *Escherichia coli* populations consisting of differing mixtures of susceptible and resistant individuals harboring CRISPR immunity to the phage. Using both experiments and mathematical modelling we describe the conditions under which herd immunity arises in bacterial populations. Notably, the effects of herd immunity depend strongly on the presence of spatial structure in the population, the bacterial growth rate, and phage replication rate. The results of our model can apply to other host–pathogen systems to determine the herd immunity threshold from the relative speed of an epidemic wave in partially resistant populations. In addition, our findings suggest that herd immunity plays an important role in bacterial communities, as seen in other host–pathogen systems, allowing for stable coexistence of bacteria and their phages and the maintenance of polymorphism in bacterial immunity.

## Introduction

“Herd immunity” has been used in a variety of ways by different authors (see [1]). Here, we define it as a phenomenon where a fraction of resistant individuals in a population reduces the probability of transmission of a pathogen among the susceptible individuals. Furthermore, if the fraction of resistant individuals in a population is sufficiently large the spread of a pathogen is suppressed. Experimental research into the phenomenon has focused mostly on mammals [2,3], birds [4,5], and invertebrates [6,7]. In human populations the principles of herd immunity were employed to limit epidemics of pathogens through vaccination programs [1], which in the case of smallpox lead to its eradication between 1959 and 1977 [8].

Alongside advances in vaccination programs, the formalization of a general theory of herd immunity was developed. The theory is based on a central parameter,  $R_0$ , which describes the fitness of the pathogen, as measured by the number of subsequent cases that arise from one infected individual in a population (for a historical review of  $R_0$  see [9]). Thus,  $R_0$  indicates the epidemic spreading potential in a population. Given  $R_0$  the herd immunity threshold is defined as,

$$H = \frac{R_0 - 1}{R_0}, \quad (1)$$

which determines the required minimum fraction of resistant individuals needed to halt the spread of an epidemic and is effected by the specific details of transmission and the contact rate among individuals [10]. Many theoretical studies have addressed the influence of some of these details, in particular maternal immunity [11], age at vaccination [12,13], age related or seasonal differences in contact rates [14–16], social structure [17], geographic heterogeneity [18–20], and the underlying contact network of individuals [21].

Interestingly, little work has focused on the potential role of herd immunity in microbial systems which contain a number of immune defense systems and have an abundance of phage pathogens. These defenses vary in their potential to provide herd immunity as they target various stages of the phage life cycle, from adsorption to replication and lysis. Early defense mechanisms include the prevention of phage

adsorption by blocking of phage receptors [22], production of an extracellular matrix [23,24], or the excretion of competitive inhibitors [25]. Alongside these bacteria have evolved innate immune systems that target phage genomes for destruction. These include host restriction-modification systems (RMS) [26], argonaute-based RNAi-like systems [27], and bacteriophage-exclusion (BREX) systems [28]. In addition to innate systems, bacteria have evolved an adaptive immune system called CRISPR-Cas (clustered regularly interspaced short palindromic repeat) [29]. In order for any of these immune systems to provide herd immunity, they must prevent further spread of the pathogen, i.e., provide a ‘sink’ for the infectious particles reducing the average number of successful additional infections below one. Unlike the early defense mechanisms that may simply prevent an infection but not the further reproduction of infectious particles, the RMS, BREX, argonaute-based RNAi-like, and the CRISPR-Cas systems degrade foreign phage DNA after it is injected into the cell, and thus continue to remove phage particles from the environment, which increases their potential to provide herd immunity. Among these the CRISPR-Cas system is unique in that it is adaptive allowing cells to acquire immunity upon infection (see Fig. 1A, B, and C), which can lead to polymorphism in immunity and give rise to herd immunity.

**Fig 1. Mechanism of CRISPR/Cas type II immunity.** The CRISPR/Cas system provides immunity to phages and its main features can be described by three distinct stages. (A) Acquisition. When a cell gets infected by a phage, a protospacer on the invading phage DNA (indicated as a red bar) is recognized by Cas1 and Cas2. The protospacer is cleaved out and ligated to the leader end (proximal to the Cas genes) of the CRISPR array as a newly acquired spacer (red diamond). (B) Processing. The CRISPR array is transcribed as a Pre-crRNA and processed by Cas9 (assisted by RNaseIII and trans-activating RNA, not shown) into mature crRNAs. (C) Interference. Mature crRNAs associate with Cas9 proteins to form interference complexes which are guided by sequence complementarity between the crRNAs and protospacers to cleave invading DNA of phages whose protospacers have been previously incorporated into the CRISPR array. (D) A truncated version of the CRISPR system on a low copy plasmid, which was used in this study lacks *cas1* and *cas2* genes and was engineered to target a protospacer on the T7 phage chromosome to provide *Escherichia coli* cells with immunity to the phage. The susceptible strain contains the same plasmid except the spacer does not target the T7 phage chromosome.

In addition to immune system-specific factors, the reproductive rate of phage depends strongly on the physiology of the host bacterium [30], and the underlying effective contact network which may vary greatly in bacterial populations depending on the details of their habitat. Thus, herd immunity will be influenced by the physiological

state of the bacteria and the mobility of the phage in the environment through passive diffusion and movement of infected individuals. Taken together these details call into question the applicability of the traditional models of herd immunity from vertebrates to phage-bacterial systems. Thus, experimental investigation and further development of extended models that take into account the specifics of microbial systems are required.

To investigate under which conditions herd immunity may arise in bacterial populations, we constructed an experimental system consisting of T7 phage and bacterial strains susceptible and resistant to it. Our experimental system can be characterized by the following features. First, we used two strains of *Escherichia coli*, one with an engineered CRISPR-based immunity to the T7 phage, and the other lacking it (Fig. 1D). Second, we examined the dynamics of the phage spread in different environments – spatially structured and without structure. Furthermore, we developed and analyzed a spatially explicit model of our experimental system to determine the biologically relevant parameters necessary for bacterial populations to exhibit herd immunity.

## Results

### Properties of resistant individuals

We engineered a resistant *E. coli* strain by introducing the CRISPR-Cas Type II system from *Streptococcus pyogenes* with a spacer targeting the T7 phage genome (see Material and Methods). We further characterized the ability of the system to confer resistance to the phage. We find a significant level of resistance as measured by the probability of cell burst when exposed to T7 (Fig. 2A). However, resistance is not fully penetrant as approximately 1 in 1000 resistant cells succumb to infection. In addition, we observe that as phage load increases (multiplicity of infection, MOI) the probability that a cell bursts increases (Fig. 2A). In order to determine the herd immunity threshold in our experimental system, we constructed the resistant strain such that upon infection the cell growth is halted, yet the cell still adsorbs and degrades phages (Fig. 2B,C). This feature is important as it prevents the action of frequency dependent selection which in naturally growing populations will favour the resistant strain until its frequency reaches

the herd immunity threshold. Thus, in our system if the frequency of the resistant strain is below the herd immunity threshold, the resistant cells remain below the threshold and are unable to stop the epidemic and the whole population collapses. In contrast, if the frequency of resistant individuals in the population is above the herd immunity threshold, the resistant individuals provide complete herd immunity and the population survives. These properties allow us to quantify the expanding epidemic in both liquid media and on bacterial lawns (without and with spatial structure, respectively) using high throughput techniques. Specifically, it allows us to control for the complex dynamics of the system arising from frequency dependent selection and simultaneous changes in the physiological states of the cells (growth rates depending on the nutrient concentrations) and phage (burst size, latent period depending on the cells' physiology).

**Fig 2. Efficiency of bacterial resistance.** (A) The probability that a resistant cell bursts, relative to a susceptible cell, at three different initial multiplicities of infection (MOI). The probability that a resistant cell bursts at MOI 1000 is significantly higher than at MOI 10 ( $p = 0.019$ ,  $t_{4,0.05} = 3.031$ ) or at MOI 100 ( $p = 0.022$ ,  $t_{5,0.05} = 2.674$ ). The error bars show the standard deviations from the mean. Note that this measure is not a widely used 'efficiency of plating' but it determines the probability of burst of single resistant cells (see Materials and Methods for details). (B) The number of colony forming units (CFUs) post phage challenge (see Materials and Methods). The mean number of CFUs after the bacterial cultures were exposed to the phage is not significantly different between susceptible and resistant strains at MOI 10 ( $p = 0.239$ ,  $t_{22,0.05} = 0.721$ ) and (C) at MOI 100 ( $p = 0.27$ ,  $t_{30,0.05} = 1.124$ ), indicating that the resistant cells' growth is halted after the cells are infected by a phage. The error bars show the standard deviations from the mean. There were no detectable CFUs in either susceptible or resistant cell cultures at MOI 1000. It should be noted that the indicated MOI values do not correspond to the average number of phages that adsorb to cells in the experiments. For MOI 10 we estimated the mean number of phages per cell as 0.229 and for MOI 100 as 0.988 (see Materials and Methods for details). It was impossible to determine the mean for MOI 1000 as there were no detectable CFUs under such conditions.

## Herd immunity in populations without spatial structure

To understand the influence of spatial population structure, or lack thereof, we first measured the probability of population survival (i.e., whether the cultures are cleared or not) in well mixed liquid environments (no spatial structure) consisting of differing proportions of resistant to susceptible individuals and T7 phage. When the percentage of resistant individuals is in excess of 99.6% all 16 replicate populations survive a phage epidemic (i.e., show no detectable difference in growth profiles to the phage free

controls; Fig. 3). Populations with 99.2% and 98.4% resistant individuals show intermediate probabilities of survival – 10 out of 16 replicate populations and 4 out of 16 replicate populations survive, respectively (Fig. 3). The likely explanation as to why some populations survive and others collapse is due to the stochastic nature of phage adsorption after inoculation: If the population composition is close to the herd immunity threshold a stochastic excess of phage particles adsorbing to susceptible cells may trigger an epidemic, whereas if chance increases the number of phages adsorbing to resistant individuals, the epidemic is suppressed. However, when populations have fewer than 96.9% resistant individuals all 16 replicate populations fail to survive and collapse under the epidemic (Fig. 3).

**Fig 3. Fraction of surviving populations at 18 h post phage infection.**

Bacterial populations consisting of various fractions of resistant to susceptible individuals infected with  $\approx 50$  phages, corresponding to a multiplicity of infection (MOI) of  $\approx 10^{-4}$ , to resemble an epidemic initiated by the burst size from one infected individual (see Table 2 for burst size estimates). Each population phage challenge is replicated 16 times. The solid dark green line shows the model prediction, Eqn. (4), for the herd immunity threshold ( $H$ ), given latent period ( $\lambda$ ), bacterial growth rate ( $\alpha$ ), and phage burst size ( $\beta$ ). Shaded area indicates  $\pm 1$  standard deviation.

As mentioned in the introduction, phage and bacterial physiology may affect the herd immunity threshold. To test this we altered bacterial growth by reducing the concentration of nutrients in the medium (Fig. S1) which concurrently alters the T7 phage's latent period and burst size (Fig. 4A,B and Table 2). Indeed, we observe as bacterial growth rates decline the fraction of resistant individuals necessary for population survival decreases (Fig. 4C). When the populations are grown in a 50% diluted growth medium, the fraction of resistant individuals required for a 100% probability of survival is 99.2%; when the fraction of resistant individuals is 75% or less populations go extinct. In a 20% growth medium the fraction of resistant individuals required for survival decreases to 96.9%, while the fraction when all replicates collapse to 50%.

From the experimental observations of the herd immunity threshold values we infer the phage  $R_0$  using Eqn. 1. In an undiluted growth medium the phage  $R_0$  falls between 32 and 256 and decreases to between 4 and 128 in 50% and between 2 and 32 in 20% nutrient medium. These data indicate that bacterial populations can exhibit herd immunity in homogeneous liquid environments. However, bacteria typically live in

**Fig 4. Herd immunity threshold in liquid culture as a function of bacterial growth.** (A) Phage burst size ( $\beta$ ) change as a function of nutrient concentrations. Brown dashed line shows a numerical quadratic fit to the observed values of  $\beta$ . (B) Latent period ( $\lambda$ ) increase across the range of nutrient concentrations. Values for  $\beta$  and  $\lambda$  are given in Table 2. (C) Population survival analysis upon phage challenge as a function of the fraction of resistant cells and the intrinsic growth rate (nutrient availability,  $N$ ). The empty circles, circled dots, and filled circles represent the outcomes of 18 replicates done in 3 independent batches, as indicated in the legend. The green line shows the model predicted herd immunity threshold given by Eqn. (5), using a quadratic fit for  $\beta/\lambda$  and inverting the Monod kinetics of bacterial growth (see Fig. S1B) numerically. Light green error-bars are estimates from Eqn. (5) using actual experimental results for growth parameters.

spatially structured environments such as surfaces, biofilms or micro-colonies, therefore we extended our experiments to consider the potential impact of spatially structured populations.

## Herd immunity in spatially structured populations

In order to discern the role, if any, spatial structure plays in herd immunity we conducted a set of experiments in spatially structured bacterial lawns on agar plates. Spatially structured bacterial populations provide a more fine grained measure of herd immunity, compared to the population survival assays done in liquid culture. On bacterial lawns, phages spread radially from a single infectious phage particle and the radius of plaque growth on different proportions of resistant to susceptible individuals can be easily quantified. In addition, these data allow for estimating the speed of the epidemic wave front in these different regimes using real-time imaging (Fig. 5A).

**Fig 5. Properties of expanding phage epidemics on bacterial lawns.** (A) Example of plaque morphology and size change over 48 hours for populations with 50% resistant cells (top) and a control with 100% susceptible cells (bottom). (B) Mean plaque size area through time. Colors indicate the different fraction of resistant individuals (color coding as in panel C). Note the distinct two phases of plaque growth – initially, phage grow fast with exponentially growing bacteria but slow once the nutrients are depleted ( $\approx 10$  hours). The plaque radius is reduced, relative to 100% susceptible population, even when only a small fraction of resistant individuals are in the population. (C) Final plaque radius at 48 hpi. Green line shows the prediction from the model for the plaque radius  $r$ . Grey numbers indicate the number of plaques measured. Error bars indicate the standard deviations.

We observe a decline in the number of plaque forming units (data not shown) and a significant decrease in final plaque sizes as the proportion of resistant individuals in the populations increases (Fig. 5B,C). A reduction in the final plaque size compared to a

fully susceptible population was statistically significant with as few as 10% resistant individuals in a population ( $p = 0.004$ ,  $t_{53,0.05} = 2.744$ ). In order to determine the effect of resistant individuals during the earlier phase of bacterial growth (until the bacterial density on the agar plate reaches saturation; Fig. S1A), we analyze the velocities of plaque growth between 0 and 24 hours post inoculation (*hpi*). We find that the speed is significantly reduced after 11 *hpi* when the population consists of as few as 10% of resistant individuals ( $p = 0.0317$ ,  $t_{32,0.05} = 1.923$ ). As the fraction of resistant individuals further increases, the speed declines significantly at earlier and earlier time points: 6 *hpi* with 20% ( $p = 0.0392$ ,  $t_{62,0.05} = 1.79$ ), and 5.67 *hpi* with 30% ( $p = 0.0286$ ,  $t_{53,0.05} = 1.943$ ). In fact, when the fraction of resistant individuals exceeds 40%, the reduction in the speed of the spread is statistically significant immediately after the plaques are visually detectable (Fig. 6). It should be noted that all populations with such low percentages of resistant individuals in liquid environment collapsed, indicating that spatial structure significantly facilitates herd immunity.

**Fig 6. Speed of phage epidemic expansion on bacterial lawns.** (A) Speed of expanding phage epidemics for all population compositions is initially high, before it drops once nutrients are depleted at around 10 *hpi* (hours post infection). (B) Plaque speed significance. Comparing velocities of plaque spread with the 100% susceptible control. Linear regression of a sliding window spanning 4 hours of the radius sizes was calculated for all individual plaques and all compositions of the populations between  $t_0$  and  $t_{24}$ . Slopes of the linear regressions for all compositions of the populations were compared using a two-sided heteroscedastic t-test against the 100% susceptible dataset.

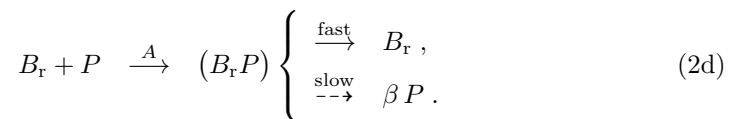
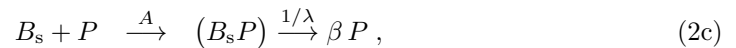
The results presented in this and the previous section would allow us to use Eq. (1) to infer a value for  $R_0$  from the observed threshold between surviving and collapsing bacterial populations, Figs. 3 and 4. We also observe that herd immunity is strongly influenced by spatial organization of the population, Fig. 5. How the exact value of  $H$  (and subsequently the “classical” epidemiological parameter  $R_0$ ) is affected by various factors such as bacterial growth rate, phage burst size and latent period is, however, difficult to resolve experimentally. Similarly, quantification of the effect of spatial structure is hardly achievable solely by experimental investigation. In order to disentangle the roles of all the factors mentioned above, we proceed with development and analysis of a mathematical model of the experimental system.



## Modelling bacterial herd immunity

We developed a model of phage growth that takes several physiological processes into account: bacterial growth during the experiment, bacterial mortality due to phage infection, and phage mortality due to bacterial immunity. Furthermore, we use the previously reported observation that phage burst size  $\beta$  and latent period  $\lambda$  depend strongly on the bacterial growth rate  $\alpha$  (see Table 1).

The main processes in our model system can be defined by the following set of reactions,



Susceptible ( $B_s$ ) and resistant ( $B_r$ ) cells grow at a rate  $\alpha$  (no significant difference in growth rate between strains,  $p = 0.066$ ,  $t_{70,0.05} = 1.867$ ), (2a) and (2b), by using an amount  $Y$  of the nutrients  $N$ . Phage infection first involves adsorption to host cells, (2c) and (2d), with the adsorption term  $A$  specified below. Infected susceptible bacteria produce on average  $\beta$  phage with a rate inversely proportional to the average latency  $\lambda$ . In contrast, resistant bacteria either survive by restricting phage DNA via their CRISPR-Cas immune system or – less likely – succumb to the phage infection. However, when the MOI is large even resistant cells become susceptible to lysis resulting in the release of phage progeny (see Fig. 2) [31, 32].

In our system, bacteria eventually deplete the available nutrients,  $N(t > T_{\text{depl}}) = 0$ , resulting in the cessation of growth. This decline in bacterial growth affects phage growth – latency increases and burst size decreases, such that phage reproduction declines dramatically (see Table 2). We define the critical time point at which cells transition from exponential growth to stationary phase as,

$$T_{\text{depl}} \approx \frac{1}{\alpha} \log \left( \frac{B_{\infty}}{B_0} \right). \quad (3)$$

Here,  $B_0$  and  $B_\infty$  are the initial and final bacterial densities, respectively. In the initial exponential growth phase, our estimates from experimental data for growth parameters are  $\alpha = 0.63 h^{-1}$ ,  $\beta = 85.6$  phages/cell and  $\lambda = 0.60 h$ , for bacteria and phages, respectively (Table 1 and Table 2). After time  $T_{\text{depl}}$ , bacterial growth rate is set to zero ( $\alpha = 0$ ) and phage growth is reduced to  $\beta_{\text{depl}} = 3.0$  phages/cell and  $\lambda_{\text{depl}} = 1.69 h$ . Such a two state model – constant growth rate while nutrients are present and no growth after depletion – describes the observed population trajectories in experiments quite well (see Fig. S1).

## Modelling herd immunity in populations without structure

An important parameter for estimating herd immunity is the fraction  $S$  of susceptible bacteria in the population. As a first estimate, a phage infection spreads in well mixed bacterial cultures if  $\beta S > 1$  for a continuous chain of infections: the product of burst size  $\beta$  of phage particles and the probability  $S$  of infecting a susceptible host has to be larger than one. As a first approximation, one could identify  $R_0$  with the burst size  $\beta$ , which is compatible with the observed herd immunity thresholds when inverting Eq. (1).

However, the growing bacterial population could outgrow the phage population, if the former reproduces faster, which introduces deviations from the simple relation between  $R_0$  and  $H$  as shown in (1). We capture this dynamical effect in a correction to the previous estimate as  $\beta S > 1 + \lambda\alpha$  (see Materials and Methods): more phages have to be produced for the chain of infections to persist in growing populations. The correction  $\frac{\lambda}{1/\alpha}$  is the ratio of generation times of phages over bacteria – usually, such a correction is very small for non-microbial hosts and can be neglected. Ultimately, herd immunity is achieved if the threshold defined by  $H = 1 - S_c$  is exceeded, with  $S_c$  the critical value in the inequality above. Rearranging, we obtain an expression for the herd immunity threshold

$$H = \frac{\beta - 1 - \lambda\alpha}{\beta} . \quad (4)$$

This estimate of  $H$  coincides to a very good extent with the population compositions of susceptible and resistant bacteria where we observe the transition from surviving and collapsed populations in experiments (see Fig. 3). Simulations presented in the Supplementary Information (section Simulation of recovery rate) show a range in the

bacterial population composition with non-monotonic trajectories for  $B_s$  and  $B_r$  (see Fig. S2B), which is comparable to the range in composition we find both outcomes, i.e., some surviving and some collapsing populations in experiments. For such parameter choices, stochastic effects could then decide the observed fates of bacteria.

As presented above, the herd immunity threshold changes when the bacterial cultures grow in a diluted growth medium. In a set of independent experiments we measured bacterial growth rate  $\alpha$ , phage burst size  $\beta$  and phage latent period  $\lambda$  under such conditions (see Fig. S1B and Table 2). From these data we estimated the dependence of the phage burst size on the bacterial growth rate,  $\beta(\alpha)$ , using a numerical quadratic fit (Fig. 4A). Similarly, we estimated the dependence of the phage latent period on the bacterial growth rate,  $\lambda(\alpha)$  (Fig. 4B). Using these estimates we calculated the expected growth rate-dependent herd immunity threshold

$$H(\alpha) = \frac{\beta(\alpha) - 1 - \lambda(\alpha)\alpha}{\beta(\alpha)}, \quad (5)$$

which gives a very good prediction of the shift in the herd immunity threshold to lower values for slower growing populations (green line in Fig. 4C). This verification of our model shows that it correctly captures the dependence of the herd immunity threshold on bacterial and phage growth parameters.

## Modelling herd immunity in spatially structured populations

The dynamics of phage spread differ between growth in unstructured (e.g., liquid) and structured (e.g., plates) populations. In order to quantify the effect of spatial structure in a population, we extend our model to include a spatial dimension. In structured populations growth is a radial expansion of phages defined by the plaque radius  $r$  and the expansion speed  $v$ , for which several authors have previously derived predictions [33–39].

We assume phage movement can be captured by a diffusion process characterized with a diffusion constant  $D$ , which we estimate in independent experiments as  $D = 1.17 (\pm 0.26) \cdot 10^{-2} \text{ mm}^2/\text{h}$  (see Materials and Methods, Fig. S3). However, we assume that only phages disperse and bacteria are immobile as the rate of bacterial diffusion does not influence the expanding plaque on timescales relevant in the

experiment. Adsorption of phages on bacteria is modeled with a adsorption constant  $\delta^*$ .  
The spreading infection will sweep across the bacterial lawn with the following speed

$$v = 2\sqrt{D\delta^*}\sqrt{\beta S - 1 - \lambda\alpha}, \quad (6)$$

which is computed in more details in the Materials and Methods. This expression (6) indicates that the population composition crucially influences the spreading speed at much lower fractions of resistant bacteria than the herd immunity threshold (4), where phage expansion stops completely. Consequently, the resulting plaque radius  $r$  decays with increasing fractions of resistants and reaches zero at  $H$ . A prediction for  $r$  can be obtained by integrating (6) over time. Using the resulting expression we estimated the adsorption constant  $\delta^*$  from the growth experiments as it is difficult in practice to measure on plates. The green line in Fig. 5B is the best fit, yielding the value  $\delta^* = 4.89(\pm 0.19) \cdot 10^{-2}$  bacteria/phage  $h$  for the adsorption constant.

Our results for spatially structured populations allows us to speculate on a general epidemiological question: If an infection is not stopped by herd immunity in a partially resistant population, by how much is its spread slowed down? By generalizing (6) we can derive a relative expansion speed, compared to a fully susceptible population,

$$v_{\text{rel}} = \sqrt{1 - \frac{1 - S}{H}}. \quad (7)$$

This expression, (7), is devoid of any (explicit) environmental conditions, which are not already contained in the herd immunity threshold  $H$  itself. Thus, it could apply to any pathogen-host system. Ultimately, this relative speed approaches zero with a universal exponent of  $1/2$ , when the fraction of resistant individuals  $1 - S$  approaches the herd immunity threshold  $H$ . However, a few caveats exist when using (7), as several conditions have to be fulfilled: Obviously, a pathogen is expected not to spread in a population exhibiting complete herd immunity – the relative speed should only hold for populations below the herd immunity threshold. Moreover, if dispersal cannot be described by diffusion, but rather dominated by large jumps [40], the diffusion approach we used for traveling waves is not applicable, and thus also renders (7) inadequate.

## Discussion

The spread of a pathogen may be halted or slowed by resistant individuals in a population and thus provide protection to susceptible individuals. This process, known as herd immunity, has been extensively studied in a wide diversity of higher organisms [2–7]. However, the role of this process has largely been ignored in microbial communities. To delve into this we set out to determine under what conditions, if any, herd immunity might arise during a phage epidemic in bacterial populations as it could have profound implications for the ecology of bacterial communities.

We show that herd immunity can occur in phage-bacterial communities and that it strongly depends on bacterial growth rates and spatial population structure. Average growth rates of bacteria in the wild have been estimated as substantially slower than in the laboratory (generation time is  $\approx 6.5$  fold longer [41]), a condition that we have shown to facilitate herd immunity. Furthermore, bacterial populations in the wild are also highly structured, as bacteria readily form micro-colonies or biofilms [42] and grow in spatially heterogeneous environments such as soil or the vertebrate gut [43], a second condition we have shown to facilitate herd immunity. These suggest that herd immunity may be fairly prevalent in low nutrient communities such as soil and oligotrophic marine environments.

In an evolutionary context, herd immunity may also impact the efficacy of selection as the selective advantage of a resistance allele will diminish as the frequency of the resistant allele in a population approaches the herd immunity threshold,  $H$ . This has two important implications. First, while complete selective sweeps result in the reduction of genetic diversity at linked loci, herd immunity may lead to only partial selective sweeps in which some diversity is maintained. Second, herd immunity has a potential to generate and maintain polymorphism at immunity loci, as has been shown for genes coding for the major histocompatibility complex (MHC) [44]. Polymorphism in CRISPR spacer contents have been demonstrated in various bacterial [45–47] and Archaeal [48] populations and communities [49–51]. While these studies primarily explain polymorphisms in CRISPR spacer content as a result of rapid simultaneous independent acquisition of new spacers, we suggest that observed polymorphisms may result from frequency-dependent selection on resistance loci arising from herd immunity.

It has also been suggested that herd immunity might favor stable coexistence between  
hosts and their pathogens [52–54].

We also developed a mathematical model and show how the herd immunity  
threshold  $H$  (Eqn. (4)) depends on the phage burst size  $\beta$  and latent period  $\lambda$ , and on  
the bacterial growth rate  $\alpha$ . This dependence arises as phages have to outgrow the  
growing bacterial population, as host and pathogen have similar generation times in our  
microbial setting. In addition to these parameters, we also describe how the speed  $v$   
(Eqn. (6)) of a phage epidemic in spatially structured populations depends on phage  
diffusion constant  $D$ , phage adsorption rate  $\delta^*$ , and the fraction of resistant and  
susceptible individuals in the population. All of which are likely to vary in natural  
populations. We also derived the relative speed of spread for partially resistant  
populations, as measured relative to a fully susceptible population, and show that it can  
be parametrized solely with the herd immunity threshold  $H$  (Eqn. (7)). This relative  
speed of the spread of an epidemic should be applicable to any spatially structured host  
population where the spread of the pathogen can be approximated by diffusion. Both  
our experiments and the modelling show that even when the fraction of resistant  
individuals in the population is below the herd immunity threshold the expansion of an  
epidemic can be substantially slowed, relative to a fully susceptible population.

In conclusion, we have presented an experimental model system and the connected  
theory that can be usefully applied to both microbial and non-microbial systems. Our  
theoretical framework can be useful for identifying critical parameters, such as  $H$  (and  
to some extent  $R_0$ ), from the relative speed of an epidemic expansion in partially  
resistant populations so long as the process of pathogen spread can be approximated by  
diffusion. This approximation has been shown to be useful in such notable cases as  
rabies in English foxes [55], potato late blight [56], foot and mouth disease in feral  
pigs [57], and malaria in humans [58].

## Materials and Methods 323

### Experimental methods 324

#### Engineering resistance 325

Oligonucleotides AACTTCGGGAAGCACTTGTGGAAG and 326  
AAACTTCCACAAGTGCTTCCCGAA were ordered from Sigma-Aldrich, annealed 327  
and ligated into pCas9 plasmid (pCas9 was a gift from Luciano Marraffini, Addgene 328  
plasmid #42876) carrying a *Streptococcus pyogenes* truncated CRISPR type II system. 329  
For the detailed protocol see [59]. The oligonucleotides were chosen so that the CRISPR 330  
system targets an overlap of phage T7 genes 4A and 4B. Therefore, the CRISPR system 331  
allows the gene 0.7, coding for a protein which inhibits the RNA polymerase of the cell, 332  
to be expressed before the T7 DNA gets cleaved [60]. The subsequent growth of the 333  
cells is halted and phage replication is inhibited. The plasmid was electroporated into 334  
*Escherichia coli* K12 MG1655 (F- lambda- *ilvG- rfb-50 rph-1*). The T7 wildtype phage 335  
was used in all experiments. 336

#### Efficiency of the CRISPR-Cas system 337

Efficiency of the engineered CRISPR-Cas system was tested using the following 338  
protocol: Overnight culture was diluted 1 in 10, cells were infected with the T7 phage 339  
and incubated for 15 min in 30°C. Cells were spun down for 2 min in room temperature 340  
at 21130g. Supernatant was discarded and the cell pellet was resuspended in 950  $\mu$ l of 341  
1X Tris-HCl buffer containing 0.4% ( $\approx 227\mu$ M) ascorbic acid pre-warmed to 43°C and 342  
incubated in this temperature for 3 min to deactivate free phage particles [61]. Cultures 343  
were serially diluted and plated using standard plaque assay protocol on a bacterial 344  
lawn of susceptible cells to detect bursting infected cells. The supernatant was tested 345  
for free phage particles, which were not detected. 346

#### Determining the mean number of phages per cell 347

The cultures that were plated using standard plaque assays in the “Efficiency of the 348  
CRISPR-Cas system” experiment were also plated on LB agar plates containing 25 349  
 $\mu$ g/ml chloramphenicol to determine the number of surviving CFUs. The numbers of 350

bursting and surviving susceptible cells were subsequently used to determine the actual mean number of adsorbed phages per cell. The fraction of susceptible cells surviving the phage challenge experiment was assumed to correspond to the Poisson probability that a cell does not encounter any phage, which was then used to determine the mean of the Poisson distribution, which corresponds to the mean number of phages per cell.

### Herd immunity in a liquid culture

Herd immunity in a liquid culture was tested in 200  $\mu\text{l}$  of LB broth supplemented with 25  $\mu\text{g/ml}$  chloramphenicol in Nunclon flat bottom 96 well plate in a Bio-Tek Synergy H1 Plate reader. Bacterial cultures were diluted 1 in 1000 and mixed in the following ratios of resistant to susceptible cells: 50:50, 75:25, 87.5:12.5, 93.75:6.25, 96.88:3.13, 98.44:1.56, 99.22:0.78, 99.61:0.39, 99.8:0.2, 99.9:0.1, 99.95:0.05, 100:0 %. T7 phage was added at a multiplicity of infection (MOI) of  $\approx 10^{-4}$  ( $\approx 50$  plaque forming units (*pfu*) per culture) to resemble an epidemic initiated by the burst size from one infected cell and the cultures were monitored at an optical density 600 nm for 18 hours post inoculation (*hpi*).

### Time-lapse imaging of plaque growth

Soft LB agar (0.7%) containing 25  $\mu\text{g/ml}$  chloramphenicol was melted and poured into glass test tubes heated to 43°C in a heating block. After the temperature equilibrated, 0.9 ml of a bacterial culture consisting of resistant and susceptible cells (ratios 10% – 100% of susceptible cells, 10% increments) were diluted 1 in 10 and added to the tubes. Then, 100  $\mu\text{l}$  of bacteriophage stock, diluted such that there would be  $\approx 10$  plaques per plate, was added to the solution. Tubes were vortexed thoroughly and poured as an overlay on LB agar plates containing 25  $\mu\text{g/ml}$  chloramphenicol. The plates were placed on scanners (Epson Perfection V600 Photo Scanner) and scanned every 20 minutes in "Wide Transparency mode" for 48 hours. A total of 3 scanners were employed with a total of 12 plates, plus a no phage control plate and 100% resistant control outside the scanners (see Fig. S4). Time-lapse images were used to calculate the increase of individual plaque areas using image analysis software PerkinElmer Velocity v6.3.



### Bacterial growth on soft agar

Growth rate of susceptible bacteria in soft LB agar (0.7%) was measured by sampling from a petri dish with a soft agar overlay with bacteria prepared in the same way as the plaque assays except an absence of the phage. Sampling was performed in spatially randomized quadruplicates at the beginning of the experiment and subsequently after 2, 4, 6, 8, 10, 12, 14, 16, 24, 32, 40, and 48 hours using sterile glass Pasteur pipettes (Fisherbrand art.no.: FB50251). Samples were blown out from the Pasteur pipette using an Accu-jet pro pipettor into 1 ml of M9 buffer pre-warmed to 43°C, vortexed for 15 seconds and incubated for 10 minutes in 43°C with two more vortexing steps after 5 and 10 minutes of incubation. Samples were serially diluted and plated on LB agar plates containing 25 µg/ml chloramphenicol. How bacterial densities change over time, measured as CFU/ml, is shown in Fig. S1A.

### Bacterial growth rates in liquid culture

	<i>Estimate</i>	<i>Units</i>
$\alpha_{\max}$	0.720 ( $\pm 0.011$ )	$[h^{-1}]$
$K_c$	0.257 ( $\pm 0.012$ )	Dilution $N$ of LB $[0 \dots 1]$

**Table 1. Estimated parameters for bacterial growth using Monod kinetics.** Undiluted LB medium ( $N = 1$ ) is assumed to have 15 mg/ml nutrients (10 mg/ml Tryptone, 5 mg/ml yeast extract). The full dataset is shown in Fig. S1.

Nutrient-dependent growth rate of susceptible bacteria was measured in Nunclon flat bottom 96 well plate in Bio-Tek Synergy H1 Plate reader in 30°C. Overnight LB cultures were diluted 1:200 in media consisting of LB broth mixed with 1X M9 salts in ratios 10:90, 20:80, 30:70, 40:60, 50:50, 60:40, 70:30, 80:20, 90:10 and 100:0. Final volume was 200 µl. Optical density at 600 nm was measured every 10 min. Natural logarithm of the optical density values was calculated to determine the growth rate using a maximal slope of a linear regression of a sliding window spanning 90 min.

The resulting growth rates for various nutrient concentrations fit well with Monod's growth kinetics,

$$\alpha = \alpha_{\max} \frac{N}{K_c + N} \quad (8)$$

Results for the two fitting parameters,  $\alpha_{\max}$  and  $K_c$ , are listed in Table 1. The whole dataset, including the fit, is displayed in Fig. S1B.

Medium	Dilution $N$	Latent period $\lambda$ [min]	Burst size $\beta$	Burst size/hour $\beta/\lambda$ [ $h^{-1}$ ]
LB 0	0.0	101.1 ( $\pm 10.9$ )	3.0 ( $\pm 1.9$ )	1.8 ( $\pm 1.1$ )
LB 20	0.2	43.4 ( $\pm 3.9$ )	12.0 ( $\pm 4.2$ )	16.6 ( $\pm 6.0$ )
LB 50	0.5	40.0 ( $\pm 3.0$ )	35.6 ( $\pm 16.4$ )	53.4 ( $\pm 24.9$ )
LB 100	1.0	36.1 ( $\pm 6.1$ )	85.6 ( $\pm 47.3$ )	142.1 ( $\pm 82.1$ )

**Table 2. Estimated parameters for phage growth.** See also Fig. 4A,B.

Test for a difference in growth rates of resistant and susceptible bacteria was done in LB broth in the same manner as nutrient-dependent growth rate measurements. Two-sample t-test was performed on acquired growth rate data.

All growth media used in growth rate measurements were supplemented with 25  $\mu g/ml$  chloramphenicol.

### Phage burst sizes

Phage burst sizes in bacteria growing at different growth rates were measured by one-step phage growth experiments. The burst sizes were calculated as the ratio of average number of plaque before burst to average number of plaques after burst. Consecutive samplings before and after burst were used for the calculation if they were not significantly different from each other (two sided t-test,  $p > 0.05$ ).

### Phage latent periods

Phage latent periods were determined as the time interval between the first and the last significantly different consecutive samplings between those used for phage burst size calculations.

### Phage diffusion in soft agar

Soft M9 salts soft agar (0.5%) was supplemented with SYBR safe staining (final conc. 1%) and poured into glass cuvettes (VWR type 6040-OG) to fill  $\sim 2$  cm of the cuvette height. After soft agar solidification, the same stained soft agar was supplemented with T7 phage particles to a final concentration  $10^{11}$  pfu/ml and poured on top of the agar without phages. The cuvettes were monitored in  $30^\circ C$  every hour for 40 hours at the SYBR safe emission spectrum peak wave length 524 nm illuminated with the SYBR safe excitation spectrum peak wave length 509 nm. The diffusion constant was estimated as

the best fit parameter for the spread of fluorescent phages through the soft agar over 426  
time. 427

First we computed the luminosity  $L_i$  of fluorescence (a gray-scale value defined as 428  
 $L = 0.2126R + 0.7152G + 0.0722B$  from the RGB image) as average over the width of 429  
the cuvette for pixel row  $i$ , and corrected the profiles of luminosity  $L_i$  by subtracting 430  
the background value. This background value was estimated as a linear fit at the end of 431  
the profile without phages, where only the gray value of the agar was measured. 432  
Moreover, luminosity saturates at values above  $\sim 0.4$  where it does not have a simple 433  
linear dependence on fluorescence: diffusion would lead to a decrease of the signal 434  
behind the inflection point of the profile and increase after the inflection point, but 435  
images only show increasing profiles – the bulk density does not decay. Thus, any 436  
estimate should only take the part of the profile that is below the threshold value of 0.4 437  
into account (see Fig. S3). 438

The diffusion constant  $D$  itself was estimated as the minimal value of the total 439  
squared deviation of the convoluted profile  $L^{(t)}$  (at time  $t$ ) with a heat kernel  $K(D)$  440  
compared to the profile  $L^{(t+1)}$  at time  $t + 1$ , 441

$$D = \left\langle \min_D \sum_i \left( \left( \sum_j \frac{e^{-(i-j)^2/4D}}{\sqrt{4\pi D}} L_j^{(t)} \right) - L_i^{(t+1)} \right)^2 \right\rangle. \quad (9)$$

Such a convolution with the heat kernel  $K_{ij}(D) = (4\pi D)^{-1/2} \exp(-(i-j)^2/4D)$  442  
assumes that the only change in the profile is due to diffusion for a time span of length 443  
1 with  $i$  and  $j$  indices of pixels. Thus, expression (9) estimates the diffusion constant in 444  
units of  $\text{pixel}^2/\text{frame}$ , where frame is the time difference between two images. Several 445  
estimates are averaged over different snapshots in the whole experiment that spans 40  $h$  446  
in intervals of 1  $h$  each. 447

The final estimate in appropriate units is 448

$$D \approx 1.17 (\pm 0.26) \cdot 10^{-2} \text{ mm}^2/h, \quad (10)$$

which is in agreement with previous measures of phage diffusion [62–64]. 449

## Modelling 450

### Phage growth 451

In the main text we stated that relevant processes for phages growing on bacteria are given by the set of reactions (2). In the following, we will analyze an extended version of our model, which takes all these processes into account. We try to justify our approximations and explain the reasoning behind leaving parts of the full model out. While reactions for single bacteria or phages are inherently stochastic in nature, we assume that the involved numbers are large enough such that the dynamics can be described with deterministic differential equations for the populations. Furthermore, reaction rates are identified with the inverse of the average time scale of the process. Thus, the full model is given by the coupled differential equations, 460

$$\partial_t B_s = \alpha B_s - A[B_s, P|B_j], \quad (11a)$$

$$\partial_t B_r = \alpha B_r - A[B_r, P|B_j] + \rho I_r, \quad (11b)$$

$$\partial_t I_s = A[B_s, P|B_j] - (1/\lambda) I_s, \quad (11c)$$

$$\partial_t I_r = A[B_r, P|B_j] - (1/\lambda) I_r - \rho I_r, \quad (11d)$$

$$\partial_t P = (\beta/\lambda)(I_s + I_r) - \sum_{i \in \{s,r\}} A[B_i, P|B_j] - \sum_{i \in \{s,r\}} A[I_i, P|B_j], \quad (11e)$$

$$\partial_t N = -\alpha/Y(B_s + B_r). \quad (11f)$$

Both bacterial populations  $B_i$  grow with rate  $\alpha$  and decay via adsorption of phages  $A[B_i, P|B_j]$ , an expression that is specified below. Infected populations  $I_i$  gain numbers by adsorption and decrease via bursting. Resistant bacteria also can recover from their infected state with a recovery rate  $\rho$ . Phages grow by bursting cells, and lose numbers by adsorption to the various bacterial populations. Moreover, explicit dynamics for nutrients is considered, which are drained by each grown cell inversely proportional to the yield  $Y$ , the conversion factor between nutrient concentration and cell numbers. Essentially, this last equation acts as a timer, when we switch from abundant resources to the depleted state: all growth parameters change significantly upon nutrient depletion. Nevertheless, despite the possible deviations, we assume depletion time is given by the simple estimate (3) and only treat the two possible states of abundant and 471

depleted nutrients. 472

Adsorption of phages, given by the term  $A[B_i, P|B_j]$ , can be influenced by the whole 473  
distribution of populations within the culture. In liquid medium, a common assumption 474  
is that this term is proportional to the concentrations of both the phages and cells [65], 475

$$A[B_i, P|B_j] = \delta B_i P, \quad (12)$$

with an adsorption constant  $\delta$ . This expression assumes constant mixing of the 476  
population and relatively short contact times between phages and bacteria. In general, 477  
this system of equations is akin to Lotka-Volterra dynamics, which has been analyzed in 478  
great detail, eg. [66, 67]. 479

For our ensuing analysis, we neglect the population of infected resistant bacteria  $I_r$ . 480  
Upon examining (11d) we find that most cells to leave their infected state by reducing 481  
phage DNA via CRISPR/Cas instead of bursting if  $\rho \gg 1/\lambda$ . If furthermore  $\rho \gg \delta P$ , 482  
which is true at least in the initial stages of the experiment, essentially all infected 483  
resistant bacteria immediately recover from a phage infection. Consequently, with both 484  
conditions, the resistant infected bacteria tend to vanish,  $I_r \rightarrow 0$ , and their dynamics 485  
can be neglected. Only in the Supplementary Information (section Simulation of 486  
recovery rate) we release this assumption to explicitly cover the full dynamics of (11) in 487  
simulations to estimate values for  $\rho$ . 488

### Exponentially growing bacteria lead to double exponential phage growth 489

For convenience, we transform the populations to the total bacterial density 490  
 $B = B_s + B_r$  and introduce the fraction of susceptible cells  $S = B_s/B$ . The crucial 491  
assumption for the remainder of this section is that phages burst immediately after 492  
infection,  $\lambda = 0$ , such that we can ignore all infected populations. While not a very 493  
biological condition, it allows to analyze the model in more detail. Using these 494  
simplifications, we obtain 495

$$\partial_t B = (\alpha - \delta SP)B, \quad (13a)$$

$$\partial_t S = -S(1 - S)\delta P, \quad (13b)$$

$$\partial_t P = (\beta S - 1)\delta BP. \quad (13c)$$

If we assume that in initial stages of phage growth the number of phages is small, ie. 496  
 $\delta P \ll \alpha \sim \mathcal{O}(1 h^{-1})$ , the dynamics of bacteria and the fraction of susceptibles simplify 497  
to  $\partial_t B = \alpha B$  and  $\partial_t S = 0$ . Note that this term  $\delta P$  also occurs in the linear phage 498  
dynamics, where it cannot be neglected. In this instance, we need to view  $\delta B$  as a 499  
coefficient, which is likely much larger initially. This set of simplified equations can be 500  
solved in closed form, 501

$$S(t) = S_0, \quad (14a)$$

$$B(t) = B_0 \exp(\alpha t), \quad (14b)$$

$$P(t) = P_0 \exp((S_0 \beta - 1) \delta B_0 (\exp(\alpha t) - 1) / \alpha). \quad (14c)$$

The structure of phage dynamics is particularly important here – it exhibits a 502  
double-exponential dependence on time  $t$ , which is a very fast, almost explosive, growth. 503  
Such double-exponential growth leads to very large population sizes within a short 504  
amount of time (but after an extended initial delay). This general behavior of the 505  
solution is independent of the actual growth rate of phages, which only has to be 506  
positive. Thus, inspecting the exponent in (14c) yields the condition 507

$$\beta S_0 > 1 \quad (15)$$

for phage growth to be positive. Incidentally, relation (15) is the naive estimate for the 508  
number of successful additional infections arising from a single burst. The double 509  
exponential time-dependence is central for our arguing that the dynamics can be 510  
described by threshold phenomena, given by conditions like (15): Usually, phages are 511  
negligible in the dynamics until they grow fast enough to large enough size, such that it 512  
is too late for the bacterial population to deal with the overwhelming phage population. 513

An important question in the context of these solutions is whether nutrients run out 514  
before this double-exponential growth of phages occurs. Hence, we compute the time  $T_\delta$  515  
defined as when phages reach a population of  $P(T_\delta) = 1/\delta$  assuming phages grow as 516  
(14c) until then. After  $T_\delta$  the assumptions that allowed to obtain (14c) are not valid 517

anymore. Inverting (14c) for time leads to

$$T_{\delta} = \frac{1}{\alpha} \log \left( 1 + \frac{\alpha \log(1/\delta P_0)}{(\beta S_0 - 1)\delta B_0} \right). \quad (16)$$

Subsequently, we can compare this estimate  $T_{\delta}$  to the depletion time

$T_{\text{depl}} = (1/\alpha) \log(B_{\infty}/B_0)$ . When rearranging the inequality  $T_{\text{depl}} > T_{\delta}$  in terms of the (initial) fraction of susceptibles  $S_0$ , we obtain

$$\beta S_0 > 1 + \frac{\alpha \log(1/\delta P_0)}{\delta(B_{\infty} - B_0)}. \quad (17)$$

This expression (17) is a condition for phages to reach “large” population sizes before nutrients are depleted by bacteria. The final population density  $B_{\infty}$  usually fulfills  $\delta B_{\infty} \gg 1$ , such that the correction given by the second term of (17) can be considered small. Thus, if phages grow ( $\beta S_0 > 1$ ), they also grow very fast with a double-exponential time-dependence and reach a considerably large population size before bacteria stop multiplying (for almost all parameter values).

### Extending analysis to finite burst times

The analysis above only treated the case  $\lambda \rightarrow 0$ . However, we reported that the latency time  $\lambda$  increases significantly when bacterial growth rate  $\alpha$  declines, see Table 2.

Considering finite latency times entails dealing with an infected bacterial population  $I$ . (However, we identify  $I \equiv I_s$  and set  $I_r = 0$ .)

To this end, note that we can rearrange (11a) to  $(1 + \lambda \partial_t)I = \lambda \delta S B P$  using the adsorption model in (12). Hence, we can use the differential operator  $(1 + \lambda \partial_t)$  and apply it directly to (11e) to reduce the dependence on  $I$  in this equation at the cost of introducing higher order derivatives. In particular, we obtain

$$\lambda \partial_t^2 P + (1 + \lambda \delta B) \partial_t P + \delta B (\beta S - 1 - \lambda \alpha) P = 0, \quad (18)$$

where we also inserted  $\partial_t B \approx \alpha B$  in the last term, as we aim again for a solution at initial times where  $\delta P \ll \alpha$ . The effects of the limit  $\lambda \rightarrow 0$  are directly observable – no terms are undefined in this limit. In particular, we find that equation (18) and  $\lambda = 0$  lead directly to the dynamics of phages we just analyzed above, obtaining solution (14c).

In principle, (18) is a hyperbolic reaction-diffusion-equation, which is known to occur upon transformation (or approximation) of time-delayed differential equations [68]. For initial times we can use the solutions  $B(t) = B_0 \exp(\alpha t)$  and  $S(t) = S_0$ . To proceed, we introduce the auxiliary variable

$$z(t) = -\delta B_0 \exp(\alpha t) / \alpha, \quad (19)$$

and assume  $P(z)$  as a function of this new variable  $z$ . We need to transform the differential operators of time derivatives, and obtain  $\partial_t = \frac{\partial z(t)}{\partial t} \partial_z = \alpha z \partial_z$  and  $\partial_t^2 = (\alpha z \partial_z)(\alpha z \partial_z) = \alpha^2 (z \partial_z + z^2 \partial_z^2)$ . Inserting these expressions in (18) and multiplying the whole equation with  $(\alpha^2 \lambda z)^{-1}$  yields the dynamics for phages,

$$0 = z \partial_z^2 P(z) + (b - z) \partial_z P(z) - a P(z), \quad (20)$$

where the two extant constants are  $a = 1 - (\beta S_0 - 1) / (\lambda \alpha)$  and  $b = 1 + 1 / (\lambda \alpha)$ . Equation (20) is called “Kummers equation” with confluent hypergeometric functions  ${}_1F_1$  as solutions [69, pg. 504],

$$P(z) = A {}_1F_1(a, b; z) + B z^{1-b} {}_1F_1(a - b + 1, 2 - b; z). \quad (21)$$

The two integration constants  $A$  and  $B$  can be determined via the initial conditions  $P(t = 0) = P_0$  and  $(\partial_t P)(t = 0) = -\delta B_0 P_0$ . Using these conditions, the shape of the solution is again similar to before with  $\lambda = 0$  (double exponential time-dependence), although  $\lambda > 0$  introduces some skew. The most important aspect of this solution (21) is to compute the parameter combination where it switches from a decreasing to increasing function over time. A careful analysis reveals that at the parameter value  $a = 0$  the behavior of the solution changes. Consequently, we find the condition for growing phage populations,

$$\beta S_0 > 1 + \lambda \alpha, \quad (22)$$

which is a non-trivial extension including finite latency times  $\lambda$ .

Note, however, that this relation (22) does not indicate a correction to the general epidemiological parameter  $R_0$ , which can be identified with  $\beta$  in our model. Rather, it



shows that a growing bacterial population requires the phage population to grow even faster for a continuous chain of infections in an epidemic. The term  $\lambda\alpha$  denotes the ratio of generation times of pathogen over host, which in most cases is small and negligible compared to 1. For bacteria and phages, however, which have similar generation times, such a correction is needed to describe the effects of growing host population sizes. In contrast, many other epidemiological models assume the host population size constant and only pathogens are increasing (or decreasing) in number.

While our result (22) suggest that it also should hold in the limit  $\alpha \rightarrow 0$ , it might not necessarily be so. This specific limit is actually quite important for the time when nutrients are depleted in the experiments. However, at several instances in the calculations above we implied a positive  $\alpha > 0$ . The most important of these is the transformation to  $z(t) = -\delta B(t)/\alpha$ , which actually exhibits two problems: dividing by  $\alpha$  should not be allowed and  $B(t)$  is essentially constant and cannot serve as a variable in a differential equation. We also neglected the second term in  $\partial_t B = (\alpha - \delta SP)B$  throughout our calculation. For  $\alpha = 0$  this second term is dominant in bacterial dynamics and would generate non-linear phage dynamics if inserted for  $\partial_t B$  right before stating (18). However, we expect that albeit the process will run *very* slow, and might not be measurable in experiments, the simple condition  $\beta S_0 > 1$  could indicate phage expansion and bacterial decay.

### Growth of phages on plated bacterial lawn

Spatial modelling of phage expansion has produced several predictions for how plaque radius  $r$  and expansion speed  $v$  are influenced by experimentally adjustable parameters [33–39]. Here, we try to use a minimal model to estimate these two observables, based on the considerations of previous sections.

One of the main complications arises from the fact that all densities in (11) have a spatial dimension in addition to their time dependence,  $B_i = B_i(\vec{x}, t)$ ,  $i \in \{s, r\}$ . As explained in the main text we only consider phage diffusion, heterogeneities in all other densities are generated only by phage growth. The additional spatial dimension imposes a particular contact network between phages and bacteria, which are not entirely random encounters anymore: One can expect that the size of the bacterial neighborhood  $\hat{B}$  phages are able to explore is only slightly determined by the actual

density  $B$ , and can be assumed constant for most of the experiment,  $\hat{B}(B) \approx \text{const.}$  594

Consequently, the adsorption term can be written in the following way, 595

$$A[B_i, P|B_j] = \delta^* \frac{B_i}{\sum_j B_j} P, \quad (23)$$

which only depends on the *relative* frequencies of bacterial strains. The adsorption 596

constant  $\delta^*$  is both the rate of adsorption and inter-host transit time as determined by 597

the diffusion constant  $D$ . Thus, one can expect the formal dependence 598

$\delta^* = \delta^*(D, \hat{B}(B))$ . For our particular experimental setup, however,  $\delta^*$  will be treated as 599

a constant. This adsorption term (23) leads to the dynamics of phages 600

$$\partial_t P = D\nabla^2 P + G[P, S], \quad (24)$$

where we collected all contributions to phage growth in  $G[P, S]$  and added the spatial 601

diffusion term  $D\nabla^2 P$ . For simplicity, we consider only expansion in a single dimension 602

( $\nabla^2 \equiv \partial_x^2$ ), which has been found to coincide well with the dynamics of plaque 603

growth [34]. The growth term for phages is then defined as, 604

$$G[P, S] = \delta^*(S\beta - 1 - \lambda\alpha)P, \quad (25)$$

where we also consider the correction  $\lambda\alpha$  obtained from the analysis in liquid culture. 605

Reaction-diffusion equations similar to (24) have been first analyzed almost 80 years 606

ago [70, 71] and since then treated extensively, e.g. [72, 73]. They admit a traveling wave 607

solution – here, this corresponds to phages sweeping over an uninfected bacterial lawn. 608

In general, the asymptotic expansion speed for the traveling wave solutions is given by 609

the following expression, 610

$$\begin{aligned} v &= 2\sqrt{D(\partial_P G)[0, S]} \\ &= 2\sqrt{D\delta^*}\sqrt{S\beta - 1 - \lambda\alpha}. \end{aligned} \quad (26)$$

Only the linearized growth rate of phages at very low densities is relevant for the 611

expansion speed,  $\partial_P G[P = 0, S]$ . Thus, the fraction of susceptible individuals  $S$  should 612

be unchanged from its initial value  $S_0$ . It should be noted, that only for  $S_0\beta > 1 + \lambda\alpha$  613

does Eqn. (26) remain valid, otherwise we have  $v = 0$ . Such a scenario is relevant when nutrients are depleted and phage growth parameters changes to  $\beta_{\text{depl}}$  and  $\lambda_{\text{depl}}$ .

The expression for the expansion speed also shows the need for the spatial adsorption model in (23), in contrast to the liquid case (12). If adsorption would directly depend on the bacterial density  $B$ , the additional linear dependence on  $B$  in (25) would lead to an exponentially increasing speed during the experiment. This is in clear contradiction to experimental observations.

The density of phages behind the expanding front is large and as previously noted at large MOIs the CRISPR-Cas system fails to provide effective immunity (see section Efficiency of the CRISPR-Cas system and SI Infection load and efficiency of the CRISPR/Cas system). However, in comparison to an un-structured environment (e.g., liquid) the structured environment effectively limits transit of phage from within a plaque to the expanding front: The combined effect of growth and diffusion usually generates a much faster expansion of phages during plaque formation, than diffusion alone. Only when nutrients are depleted, can pure diffusion processes explain the slow decrease in speed observed in experiments (see Fig. 6A). Our model assumes a sharp drop to  $v = 0$  at  $T_{\text{depl}}$  for small  $S$ .

In order to derive an expression for the plaque radius  $r$ , we integrate the expansion speed (6) over time,  $r(t) = \int_0^t dt' v(t')$ . Employing the simplification that only two values of phage growth are necessary to describe the dynamics – before  $T_{\text{depl}}$  phages grow normally with  $\beta$  and  $\lambda$ , after  $T_{\text{depl}}$  phage growth changes to  $\beta_{\text{depl}}$  and  $\lambda_{\text{depl}}$  – we can evaluate the integral for the radius directly, arriving at,

$$r(t) = \begin{cases} 2t\sqrt{D\delta^*}\sqrt{S\beta - 1 - \lambda\alpha}, & 0 < t < T_{\text{depl}}, \\ 2\sqrt{D\delta^*}\left(T_{\text{depl}}\sqrt{S\beta - 1 - \lambda\alpha} + (t - T_{\text{depl}})\sqrt{S\beta_{\text{depl}} - 1}\right), & T_{\text{depl}} < t. \end{cases} \quad (27)$$

Using this expression we estimated the adsorption constant  $\delta^*$  from the growth experiments as it difficult to measure in practice. This estimate is done for radii exactly at the time of nutrient depletion  $T_{\text{depl}}$ , and excluding the control experiment with only susceptible cells.

Predictions of our model show a discrepancy from experimental results on plates. We independently estimated  $\beta_{\text{depl}} = 3.0$ , which results in  $H_{\text{depl}} = (\beta_{\text{depl}} - 1)/\beta_{\text{depl}} \approx 0.67$ .

Thus, all experiments with  $S > 0.33$  should exhibit expanding plaques after nutrients  
are depleted. In the experimental setup plaques stop expanding in all mixtures of  
resistant to susceptible cells ( $S \leq 0.9$ ), which would correspond to  $\beta_{\text{depl}} < 1.1$ . This  
value is, however, still within experimental accuracy of our estimates of  $\beta_{\text{depl}}$ .

## Acknowledgments

We are grateful to Remy Chait for his help and assistance with establishing our  
experimental setups and to Tobias Bergmiller for valuable insights into some specific  
experimental details. We thank Luciano Marraffini for donating us the pCas9 plasmid  
used in this study. Finally, we want to express our gratitude to Seth Barribeau, Andrea  
Betancourt, Călin Guet, Mato Lagator, Tiago Paixão and Maroš Pleška for valuable  
discussions on the manuscript.

## Author Contributions

Conceived and designed the experiments: PP JPB. Performed the experiments: PP.  
Analyzed the data: PP LG. Conceived and designed the model: PP LG JPB NHB.  
Encoded and analyzed the model: LG. Wrote the manuscript: PP LG NHB JPB.

## Supporting information 657

### Simulation of recovery rate 658

Throughout the main text we assumed that resistant bacteria are completely immune to phage infection as their CRISPR/Cas system immediately kills adsorbed phages. 659  
660

However, experimental observation suggest that for fractions close to what we predicted as herd immunity threshold, *all* bacteria eventually die. Thus, in the following section we use numerical simulations to investigate the full set of equations (11), with a particular focus on the question why the whole bacterial population goes extinct. As it turns out, this requires using finite values for the recovery rate  $\rho$  (instead of the  $\rho \rightarrow \infty$  approximation employed previously). 661  
662  
663  
664  
665  
666

A major difficulty in analyzing the full model (11) is finding appropriate parameter values. In particular, we need values for the adsorption constant  $\delta$ , the recovery rate  $\rho$  and the yield coefficient  $Y$ . Undiluted LB medium is known to support a population of  $5 \cdot 10^9$  cells/*ml*. Thus one can easily estimate  $Y$  as the inverse of this number, when nutrients are measured in units of dilutions, which we already used throughout this publication (undiluted medium corresponds to  $N = 1$ ). Parameter scans in simulations reveal that the actual value of the adsorption constant  $\delta$  does usually not influence the actual outcome (collapsed or surviving bacterial population), it only adjusts time scales. However, deviations in time scales are insignificant, even when  $\delta$  is changed by orders of magnitude,  $\delta \sim \mathcal{O}(10^{-6} \dots 10^{-8})$ . They are roughly an hour or less, which is small compared to the expected duration of the experiment that lasts a few hours. For definiteness, we use the value of  $\delta = 10^{-7} \text{ h}^{-1}$  for our simulations. That the value of the adsorption constant has only a minor impact on phage growth on bacterial cultures, is also in line with previous findings [39]. 667  
668  
669  
670  
671  
672  
673  
674  
675  
676  
677  
678  
679  
680

The most elusive parameter is the recovery rate  $\rho$ . A first indication of the value of  $\rho$  can be drawn from our experiments on bursting resistant cells, summarized in Fig. 2. As the probability for bursting resistant cells is 3 orders of magnitude smaller than for susceptible bacteria, we can use  $1/\lambda \sim \mathcal{O}(1)$  to estimate  $\rho \sim \mathcal{O}(10^3)$ . However, our results also indicate that recovery via the CRISPR/Cas system heavily depends on MOI, implying that  $\rho$  depends on the actual densities of phages and bacteria. Nevertheless, as experimental determination of recovery is complicated, even more so determining a 681  
682  
683  
684  
685  
686  
687

functional dependence on dynamically changing densities  $B$  and  $P$ , we assume that  $\rho$  is constant.

We ran parameter sweeps in simulations and compared the outcome – collapsed or surviving bacterial populations – to the observed experimental results (see Fig. 3). The best agreement of simulations and experiments was reached with  $\rho \sim \mathcal{O}(1)$ . Lower values of  $\rho$  do not allow the resistant population to recover from phage infection, while for larger values of  $\rho$ , phages are drained from the culture very fast. Such a small value of  $\rho$  is most likely related to the recovery at very large MOI, when the densities involved in the dynamics are large, which dominate the overall observed dynamics. At this time phages repeatedly infect the same bacteria and their CRISPR/Cas immune system cannot deal with such an infection load (or only too slow). Thus, we can argue that our final choice  $\rho = 1.5 h^{-1}$  is the recovery rate when the CRISPR/Cas system is heavily stressed, which is comparable to the actual burst rate  $1/\lambda$  for phages.

In Fig. S2 we show three exemplary sets of trajectories for bacteria and phage. For a tiny fraction of susceptibles,  $S = 10^{-3}$ , which is well below the herd immunity threshold (see Fig. 3), phages do not thrive on the limited number of favorable hosts and decay fast after a slight increase initially. For intermediate fractions of susceptibles,  $S = 0.04$ , we observe more complex, non-monotonic trajectories of bacterial populations. For such values of  $S$  we also observe mixed outcomes in experiments, see Fig. 3. When  $S$  is increased further ( $S = 0.06$ ), enough susceptible bacteria exists to produce enough phages and ultimately the whole bacterial population goes extinct.

The purpose of the extended model in this section was to justify the fact that phages can wipe out the whole bacterial population, which was not possible in the simplified model used in the main text. There, the resistant bacterial population was basically unaffected by phages and just acted as “sink” for phages. However, also in this extended model, we see a very similar behavior in terms of the threshold phenomena reported earlier in the manuscript.

### Infection load and efficiency of the CRISPR/Cas system

In the section Modelling we showed that positive phage growth leads eventually to a very fast increase in the phage population, that occurs before nutrients are depleted (for

Parameter		Value	Units	Comment
Bacterial growth rate	$a$	0.63	1/h	Table 1, Fig. S1
Yield	$Y$	$2 \cdot 10^{-1}$	1/cell	measured in dilution of LB
Recovery rate	$\rho$	1.5	1/h	See SI text
Adsorption constant	$\delta$	$10^{-7}$	1/(h cell)	See SI text
Diffusion constant	$D$	$1.17 \cdot 10^{-2}$	$mm^2/h$	Section Phage diffusion in soft
Burst size	$\beta$	85.6	phages/cell	Table 2, Fig. 4
Latency time	$\lambda$	0.60	h	Table 2, Fig. 4
Initial bacterial population	$B_0$	$10^5$	cells	
Initial phage population	$P_0$	10	phages	

**Table 3. Parameters used in simulations shown in Fig. S2.**

almost all realistic parameters). This behavior of the dynamics was also observed in the extended simulation model presented in the last section. Moreover, as a condition we used that the phage population reaches a size  $P \sim 1/\delta$ , which is after all arbitrary – only determines if we can employ useful simplifications and approximations to model equations. However, simulation results presented in the last section indicate that the bacterial population starts to decay soon after such a threshold  $P \sim 1/\delta$  is exceeded.

In order to proceed, we investigate the system at time  $T_\delta$  further. We assume that the phage population is large enough that it will not be degraded by the CRISPR/Cas immune system. The threat to immediate phage extinction is low at this point. The actual equations are hard to solve directly, hence we revert to simple balance equations, ignoring the dynamical component. Specifically, we compare the number of (present and eventually produced) phages to the number of infections needed to wipe out the whole population. To incorporate the effects of the bacterial immune system in resistant bacteria, we assume that they need  $M > 1$  infections before they burst and produce only  $\kappa\beta$  phages, which reduces the burst size by a (yet unspecified) factor  $0 < \kappa < 1$ .  $\kappa = 1$  implies that resistant cells produce the same number of phages as susceptible cells, while  $\kappa = 0$  indicates only cell death. Combining these considerations yields

$$\underbrace{1/\delta}_{\text{phages present}} + \underbrace{\beta S_0 B(T_\delta)}_{\text{phage production } B_s} + \underbrace{\kappa\beta(1 - S_0)B(T_\delta)}_{\text{phage production } B_r} > \underbrace{S_0 B(T_\delta)}_{\text{infections } B_s} + \underbrace{M(1 - S_0)B(T_\delta)}_{\text{infections } B_r}, \quad (28)$$

where the left side indicates the total number of phages, while the right side indicates the number of necessary infections to kill all bacteria. The number of bacteria  $B(T_\delta)$  can be estimated by inserting the time  $T_\delta$  from (17) into the exponential growth (14b).

Subsequently, we can rearrange (28), obtaining a bound on  $M$ :

738

$$M < \frac{1/\delta B(T_\delta) + S_0(\beta - 1)}{1 - S_0} + \kappa\beta. \quad (29)$$

The first term  $1/\delta B(T_\delta)$  indicates the ratio of phages to bacteria at time  $T_\delta$ , and can be considered small for non-extremal parameters compared to the other terms. This fact justifies our assumption that the actual value of  $\delta$  is not crucial. This number  $M$  might allow some insight into the effectiveness of the CRISPR/Cas immune system. For a fraction of susceptibles  $S = 0.03$ , which corresponds to the minimal value where we observe only collapsed bacterial populations in undiluted LB medium (see Figs. 3 and 4), we would obtain the relation  $M \lesssim 3 + 86\kappa$ . Thus, each resistant bacterial cell could degrade up to  $\mathcal{O}(10^1 \dots 10^2)$  phages before their CRISPR/Cas system cannot cope with the infection load anymore.

739

740

741

742

743

744

745

746

747

## References

1. Fine P, Eames K, Heymann DL. “Herd Immunity”: A Rough Guide. *Clinical Infectious Diseases*. 2011;52(7):911–916. doi:10.1093/cid/cir007.
2. Jeltsch F, Müller MS, Grimm V, Wissel C, Brandl R. Pattern formation triggered by rare events: lessons from the spread of rabies. *Proceedings of the Royal Society of London B: Biological Sciences*. 1997;264(1381):495–503. doi:10.1098/rspb.1997.0071.
3. Mariner JC, House JA, Mebus CA, Sollod AE, Chibeu D, Jones BA, et al. Rinderpest Eradication: Appropriate Technology and Social Innovations. *Science*. 2012;337(6100):1309–1312. doi:10.1126/science.1223805.
4. Boven Mv, Bouma A, Fabri THF, Katsma E, Hartog L, Koch G. Herd immunity to Newcastle disease virus in poultry by vaccination. *Avian Pathology*. 2008;37(1):1–5. doi:10.1080/03079450701772391.
5. Meister T, Lussy H, Bakonyi T, Šikutová S, Rudolf I, Vogl W, et al. Serological evidence of continuing high Usutu virus (Flaviviridae) activity and establishment



- of herd immunity in wild birds in Austria. *Veterinary Microbiology*. 2008;127(3–4):237–248. doi:10.1016/j.vetmic.2007.08.023.
6. Konrad M, Vyleta ML, Theis FJ, Stock M, Tragust S, Klatt M, et al. Social Transfer of Pathogenic Fungus Promotes Active Immunisation in Ant Colonies. *PLOS Biol*. 2012;10(4):e1001300. doi:10.1371/journal.pbio.1001300.
  7. Wang Y, Yang P, Cui F, Kang L. Altered Immunity in Crowded Locust Reduced Fungal ( *Metarhizium anisopliae* ) Pathogenesis. *PLOS Pathog*. 2013;9(1):e1003102. doi:10.1371/journal.ppat.1003102.
  8. Fenner F. Smallpox: emergence, global spread, and eradication. *History and Philosophy of the Life Sciences*. 1993;15(3):397–420.
  9. Heesterbeek JaP. A Brief History of  $R_0$  and a Recipe for its Calculation. *Acta Biotheoretica*. 2002;50(3):189–204. doi:10.1023/A:1016599411804.
  10. Grassly NC, Fraser C. Mathematical models of infectious disease transmission. *Nature Reviews Microbiology*. 2008;6(6):477–487. doi:10.1038/nrmicro1845.
  11. Anderson RM, May RM. *Infectious Diseases of Humans: Dynamics and Control*. OUP Oxford; 1992.
  12. Anderson RM, May RM. Directly transmitted infections diseases: control by vaccination. *Science*. 1982;215(4536):1053–1060. doi:10.1126/science.7063839.
  13. Nokes DJ, Anderson RM. Measles, mumps, and rubella vaccine: what coverage to block transmission? *The Lancet*. 1988;332(8624):1374.
  14. Schenzle D. An Age-Structured Model of Pre- and Post-Vaccination Measles Transmission. *Mathematical Medicine and Biology*. 1984;1(2):169–191. doi:10.1093/imammb/1.2.169.
  15. Anderson RM, May RM. Age-related changes in the rate of disease transmission: implications for the design of vaccination programmes. *The Journal of Hygiene*. 1985;94(3):365–436.

16. Yorke JA, Nathanson N, Pianigiani G, Martin J. Seasonality and the requirements for perpetuation and eradication of viruses in populations. *American Journal of Epidemiology*. 1979;109(2):103–123.
17. Fox JP, Elveback L, Scott W, Gatewood L, Ackerman E. Herd immunity: basic concept and relevance to public health immunization practices. *American Journal of Epidemiology*. 1971;94(3):179–189.
18. Anderson RM, May RM. Spatial, temporal, and genetic heterogeneity in host populations and the design of immunization programmes. *IMA journal of mathematics applied in medicine and biology*. 1984;1(3):233–266.
19. Lloyd AL, May RM. Spatial Heterogeneity in Epidemic Models. *Journal of Theoretical Biology*. 1996;179(1):1–11. doi:10.1006/jtbi.1996.0042.
20. Real LA, Biek R. Spatial dynamics and genetics of infectious diseases on heterogeneous landscapes. *Journal of The Royal Society Interface*. 2007;4(16):935–948. doi:10.1098/rsif.2007.1041.
21. Ferrari MJ, Bansal S, Meyers LA, Bjornstad ON. Network frailty and the geometry of herd immunity. *Proceedings of the Royal Society B: Biological Sciences*. 2006;273(1602):2743–2748. doi:10.1098/rspb.2006.3636.
22. Nordström K, Forsgren A. Effect of Protein A on Adsorption of Bacteriophages to *Staphylococcus aureus*. *Journal of Virology*. 1974;14(2):198–202.
23. Hammad Amm. Evaluation of alginate-encapsulated *Azotobacter chroococcum* as a phage-resistant and an effective inoculum. *Journal of Basic Microbiology*. 1998;38(1):9–16.  
doi:10.1002/(SICI)1521-4028(199803)38:1;9::AID-JOBM9;3.0.CO;2-4.
24. Sutherland IW, Hughes KA, Skillman LC, Tait K. The interaction of phage and biofilms. *FEMS microbiology letters*. 2004;232(1):1–6.
25. Destoumieux-Garzón D, Duquesne S, Peduzzi J, Goulard C, Desmadril M, Letellier L, et al. The iron–siderophore transporter FhuA is the receptor for the antimicrobial peptide microcin J25: role of the microcin Val11–Pro16  $\beta$ -hairpin

- region in the recognition mechanism. *Biochemical Journal*. 2005;389(3):869–876. doi:10.1042/BJ20042107.
26. Blumenthal RM, Cheng X. Restriction-modification systems. *Modern microbial genetics*. 2002; p. 177–225.
27. Swarts DC, Jore MM, Westra ER, Zhu Y, Janssen JH, Snijders AP, et al. DNA-guided DNA interference by a prokaryotic Argonaute. *Nature*. 2014;507(7491):258–261. doi:10.1038/nature12971.
28. Goldfarb T, Sberro H, Weinstock E, Cohen O, Doron S, Charpak-Amikam Y, et al. BREX is a novel phage resistance system widespread in microbial genomes. *The EMBO journal*. 2015;34(2):169–183. doi:10.15252/emboj.201489455.
29. Sorek R, Lawrence CM, Wiedenheft B. CRISPR-Mediated Adaptive Immune Systems in Bacteria and Archaea. *Annual Review of Biochemistry*. 2013;82(1):237–266. doi:10.1146/annurev-biochem-072911-172315.
30. Hadas H, Einav M, Fishov I, Zaritsky A. Bacteriophage T4 development depends on the physiology of its host *Escherichia coli*. *Microbiology (Reading, England)*. 1997;143 ( Pt 1):179–185.
31. Westra ER, van Houte S, Oyesiku-Blakemore S, Makin B, Broniewski JM, Best A, et al. Parasite exposure drives selective evolution of constitutive versus inducible defense. *Current Biology*. 2015;25(8):1043–1049.
32. Chabas H, van Houte S, Høyland-Kroghsbo NM, Buckling A, Westra ER; The Royal Society. Immigration of susceptible hosts triggers the evolution of alternative parasite defence strategies. *Proc R Soc B*. 2016;283(1837):20160721.
33. Kaplan DA, Naumovski L, Rothschild B, Collier RJ. Appendix: a model of plaque formation. *Gene*. 1981;13(3):221–225.
34. Yin J, McCaskill J. Replication of viruses in a growing plaque: a reaction-diffusion model. *Biophysical journal*. 1992;61(6):1540.
35. You L, Yin J. Amplification and spread of viruses in a growing plaque. *Journal of theoretical biology*. 1999;200(4):365–373.

36. Fort J, Méndez V. Time-delayed spread of viruses in growing plaques. *Physical review letters*. 2002;89(17):178101.
37. Ortega-Cejas V, Fort J, Méndez V, Campos D. Approximate solution to the speed of spreading viruses. *Physical Review E*. 2004;69(3):031909.
38. Abedon ST, Culler RR. Optimizing bacteriophage plaque fecundity. *Journal of theoretical biology*. 2007;249(3):582–592.
39. Mitarai N, Brown S, Sneppen K. Population dynamics of phage and bacteria in spatially structured habitats using Phage  $\lambda$  and *Escherichia coli*. *Journal of bacteriology*. 2016;198(12):1783–1793.
40. Hallatschek O, Fisher DS. Acceleration of evolutionary spread by long-range dispersal. *Proceedings of the National Academy of Sciences*. 2014;111(46):E4911–E4919.
41. Gibson, Wilson, Feil, Eyre-Walker. personal communication; 2016.
42. Hall-Stoodley L, Costerton JW, Stoodley P. Bacterial biofilms: from the Natural environment to infectious diseases. *Nature Reviews Microbiology*. 2004;2(2):95–108. doi:10.1038/nrmicro821.
43. Fierer N, Jackson RB. The diversity and biogeography of soil bacterial communities. *Proceedings of the National Academy of Sciences of the United States of America*. 2006;103(3):626–631. doi:10.1073/pnas.0507535103.
44. Wills C, Green DR. A Genetic Herd-Immunity Model for the Maintenance of MHC Polymorphism. *Immunological reviews*. 1995;143(1):263–292.
45. Tyson GW, Banfield JF. Rapidly evolving CRISPRs implicated in acquired resistance of microorganisms to viruses. *Environmental Microbiology*. 2008;10(1):200–207. doi:10.1111/j.1462-2920.2007.01444.x.
46. Sun CL, Thomas BC, Barrangou R, Banfield JF. Metagenomic reconstructions of bacterial CRISPR loci constrain population histories. *The ISME journal*. 2016;10(4):858–870.

47. Kuno S, Sako Y, Yoshida T. Diversification of CRISPR within coexisting genotypes in a natural population of the bloom-forming cyanobacterium *Microcystis aeruginosa*. *Microbiology*. 2014;160(5):903–916. doi:10.1099/mic.0.073494-0.
48. Held NL, Herrera A, Cadillo-Quiroz H, Whitaker RJ. CRISPR Associated Diversity within a Population of *Sulfolobus islandicus*. *PLoS ONE*. 2010;5(9). doi:10.1371/journal.pone.0012988.
49. Pride DT, Sun CL, Salzman J, Rao N, Loomer P, Armitage GC, et al. Analysis of streptococcal CRISPRs from human saliva reveals substantial sequence diversity within and between subjects over time. *Genome Research*. 2011;21(1):126–136. doi:10.1101/gr.111732.110.
50. Zhang Q, Rho M, Tang H, Doak TG, Ye Y. CRISPR-Cas systems target a diverse collection of invasive mobile genetic elements in human microbiomes. *Genome Biology*. 2013;14:R40. doi:10.1186/gb-2013-14-4-r40.
51. Andersson AF, Banfield JF. Virus Population Dynamics and Acquired Virus Resistance in Natural Microbial Communities. *Science*. 2008;320(5879):1047–1050. doi:10.1126/science.1157358.
52. Hamer WH. *Epidemic Disease in England: The Evidence of Variability and of Persistency of Type*. Bedford Press; 1906.
53. Fine PE. Herd immunity: history, theory, practice. *Epidemiologic Reviews*. 1993;15(2):265–302.
54. Childs LM, England WE, Young MJ, Weitz JS, Whitaker RJ. CRISPR-induced distributed immunity in microbial populations. *PLoS one*. 2014;9(7):e101710.
55. Murray JD, Stanley EA, Brown DL. On the Spatial Spread of Rabies among Foxes. *Proceedings of the Royal Society of London B: Biological Sciences*. 1986;229(1255):111–150. doi:10.1098/rspb.1986.0078.
56. Scherm H. On the velocity of epidemic waves in model plant disease epidemics. *Ecological Modelling*. 1996;87(1–3):217 – 222. doi:http://dx.doi.org/10.1016/0304-3800(95)00030-5.

57. Pech RP, McIlroy JC. A Model of the Velocity of Advance of Foot and Mouth Disease in Feral Pigs. *Journal of Applied Ecology*. 1990;27(2):635–650.
58. Gaudart J, Ghassani M, Mintsa J, Rachdi M, Waku J, Demongeot J. Demography and Diffusion in Epidemics: Malaria and Black Death Spread. *Acta Biotheoretica*. 2010;58(2):277–305. doi:10.1007/s10441-010-9103-z.
59. Jiang W, Bikard D, Cox D, Zhang F, Marraffini LA. RNA-guided editing of bacterial genomes using CRISPR-Cas systems. *Nature Biotechnology*. 2013;doi:10.1038/nbt.2508.
60. García LR, Molineux IJ. Rate of translocation of bacteriophage T7 DNA across the membranes of *Escherichia coli*. *Journal of Bacteriology*. 1995;177(14):4066–4076.
61. Murata A, Kitagawa K. Mechanism of Inactivation of Bacteriophage J1 by Ascorbic Acid. *Agricultural and Biological Chemistry*. 1973;37(5):1145–1151. doi:10.1271/bbb1961.37.1145.
62. Stent GS, Wollman EL. On the two-step nature of bacteriophage adsorption. *Biochimica et biophysica acta*. 1952;8:260–269.
63. Bayer M, DeBlois R. Diffusion Constant and Dimension of Bacteriophage  $\phi$ X174 as Determined by Self-Beat Laser Light Spectroscopy and Electron Microscopy. *Journal of virology*. 1974;14(4):975–980.
64. Briandet R, Lacroix-Gueu P, Renault M, Lecart S, Meylheuc T, Bidnenko E, et al. Fluorescence correlation spectroscopy to study diffusion and reaction of bacteriophages inside biofilms. *Applied and environmental microbiology*. 2008;74(7):2135–2143.
65. Weitz JS. *Quantitative Viral Ecology: Dynamics of Viruses and Their Microbial Hosts*. Princeton University Press; 2016.
66. Hofbauer J, Sigmund K. *Evolutionary games and population dynamics*. Cambridge University Press; 1998.
67. Nowak MA. *Evolutionary dynamics*. Harvard University Press; 2006.

68. Fort J, Méndez V. Wavefronts in time-delayed reaction-diffusion systems. Theory and comparison to experiment. *Reports on Progress in Physics*. 2002;65(6):895.
69. Abramowitz M, Stegun IA. Handbook of mathematical functions: with formulas, graphs, and mathematical tables. vol. 55. Courier Corporation; 1964.
70. Fisher RA. The wave of advance of advantageous genes. *Annals of Human Genetics*. 1937;7(4):355–369.
71. Kolmogorov AN, Petrovsky I, Piscounoff N. Study of the diffusion equation with growth of the quantity of matter and its application to a biology problem. *Bull Univ Moscow, Ser Int A*. 1937;1(1).
72. Murray JD. *Mathematical biology I: an introduction*, Vol. 17 of interdisciplinary applied mathematics; 2002.
73. van Saarloos W. Front propagation into unstable states. *Physics reports*. 2003;386(2):29–222.

**Fig S1. Measuring bacterial growth without phage.** (A) Trajectory of population size on agar plates over time. For modeling, we assume two states of growth (green curve): first, the bacterial population grows exponential until the time  $T_{\text{depl}}$ , when nutrients are depleted. From this time on, growth rate is assumed to be zero and the population saturates at a maximal size  $B^{\text{final}}$ . Experimental observations fit this proposed growth curve to a very good extent. After all, half of all nutrients are used up in the last generation – with generation times of less than one hour, this the switch between growth and no-growth should be fast. (B) Growth rates of bacteria in diluted medium follow closely Monod’s empirical law, given by expression (8). Fit parameters are found to be  $\alpha_{\text{max}} \approx 0.720 \text{ h}^{-1}$  and  $K_c \approx 0.257$  (with the latter in dimensionless units as dilution of LB medium), see also Table 1.

**Fig S2. Simulated trajectories for all populations in liquid culture for the extended model, including infected and recovering bacteria.** Trajectories are obtained by numerically integrating equations (11), using parameters listed in Table 3 and additionally  $N = 1$ ,  $Y = 2 \cdot 10^{-10} \text{ cells}^{-1}$ ,  $\delta = 10^{-7} \text{ h}^{-1}$  and  $\rho = 1.5 \text{ h}^{-1}$ . (A) For population compositions with a large majority of resistant cells ( $S = 10^{-3}$ ), phages get wiped out fast. (B) For intermediate  $S$  (close to parameters where we observe both, collapsed and surviving, populations, see Fig. 3), the populations exhibit a complex, non-monotonic trajectory. After fast initial growth of phages, bacterial populations decay but ultimately can recover. (C) If the fraction of susceptibles is too large ( $S = 0.06$ ), the whole bacterial population is infected and succumbs to the overwhelming phage infection. See supporting text for more detailed information.

**Fig S3. Estimating diffusion constant of phages.** (A), (B) Phage are slowly expanding on agar which can be observed via their fluorescence. Pictures are taken  $5 \text{ h}$  apart. (C) The diffusion constant  $D$  can be estimated as best-fit parameter in a *heat kernel*  $K(D)$ :  $K(D)$  propagates the fluorescence profile  $L^{(t)}$  at time  $t$  forward (via a convolution to “smear” out the signal) to the profile  $L^{(t+\Delta t)}$  at the next measured time point. The difference between the expected change and the actual profile is quantified as total squared deviation, see Eqn. (9), which we minimize to obtain  $D$ . Consequently, we can estimate the diffusion constant as  $D \approx 1.17 \cdot 10^{-2} \text{ mm}^2/\text{h}$ . The green line uses this estimated parameter  $D$  and shows the change between the profile at  $t = 10 \text{ h}$  (orange line) and the profile at  $t = 15 \text{ h}$  (light brown line), assuming diffusive spread of phages. See Materials and Methods for more information.

**Fig S4. Image of the scanner system.** Photograph of the scanner system used for time-lapse imaging of phage spread in spatially structured bacterial populations. Three scanners (Epson Perfection V600 Photo Scanner) simultaneously scanned 12 plates in total every 20 minutes in  $30^\circ\text{C}$  for 48 hours per experiment.



